Correcting QUEST Magnetic Resonance Imaging–Sensitive Free Radical Production in the Outer Retina In Vivo Does Not Correct Reduced Visual Performance in 24-Month-Old C57BL/6J Mice

Bruce A. Berkowitz,[1] Robert H. Podolsky,[2] Karen Lins Childers,[2] Robin Roberts,[1] Michael Schneider,[1] Emma Graffice,[1] Kenan Sinan,[1] Ali Berri,[1] and Lamis Harp[1]

[1]Department of Ophthalmology, Visual and Anatomical Sciences, Wayne State University School of Medicine, Detroit, Michigan, United States
[2]Beaumont Research Institute, Beaumont Health, Royal Oak, Michigan, United States

Correspondence: Bruce A. Berkowitz, Department of Ophthalmology, Visual and Anatomical Sciences, Wayne State University School of Medicine, 540 E. Canfield, Detroit, MI 48201, USA; baberko@med.wayne.edu.

Received: February 3, 2021
Accepted: April 27, 2021
Published: May 25, 2021

Citation: Berkowitz BA, Podolsky RH, Childers KL, et al. Correcting QUEST magnetic resonance imaging–sensitive free radical production in the outer retina in vivo does not correct reduced visual performance in 24-month-old C57BL/6J mice. *Invest Ophthalmol Vis Sci*. 2021;62(6):24. https://doi.org/10.1167/iovs.62.6.24

Purpose. To test the hypothesis that acutely correcting a sustained presence of outer retina free radicals measured in vivo in 24-month-old mice corrects their reduced visual performance.

Methods. Male C57BL/6J mice two and 24 months old were noninvasively evaluated for unremitted production of paramagnetic free radicals based on whether 1/T1 in retinal laminae are reduced after acute antioxidant administration (QUEnch-assiSTed [QUEST] magnetic resonance imaging [MRI]). Superoxide production was measured in freshly excised retina (lucigenin assay). Combining acute antioxidant administration with optical coherence tomography (i.e., QUEST OCT) tested for excessive free radical–induced shrinkage of the subretinal space volume. Combining antioxidant administration with optokinetic tracking tested for a contribution of uncontrolled free radical production to cone-based visual performance declines.

Results. At two months, antioxidants had no effect on 1/T1 in vivo in any retinal layer. At 24 months, antioxidants reduced 1/T1 only in superior outer retina. No age-related change in retinal superoxide production was measured ex vivo, suggesting that free radical species other than superoxide contributed to the positive QUEST MRI signal at 24 months. Also, subretinal space volume did not show evidence for age-related shrinkage and was unresponsive to antioxidants. Finally, visual performance declined with age and was not restored by antioxidants that were effective per QUEST MRI.

Conclusions. An ongoing uncontrolled production of outer retina free radicals as measured in vivo in 24 mo C57BL/6J mice appears to be insufficient to explain reductions in visual performance.

Keywords: aging, MRI, OCT, oxidative stress, rod photoreceptors

Physiological aging causes visual performance declines by an unknown and so far untreatable mechanism(s).[1] Diminished vision with age is important because it predicts fall-based injuries and long-term survival in healthy adults; it is also linked to sight-threatening age-related diseases such as age-related macular degeneration.[1–6] Intriguingly, rod photoreceptors and retinal pigment epithelium (RPE) are reported to be the initial targets affected by age.[4,7–11] Notably, rod photoreceptors and RPE participate in cone photoreceptor function via modulation of rod-cone gap junction coupling, control over light-adaptive dopamine release, and regulation of subretinal space hydration.[12–15] Thus, rod photoreceptor and RPE appear to offer a reasonable platform for noninvasive early testing for mechanisms that underlie later retina-based declines in vision.

One commonly proposed mechanism for age-related declines in vision and risk of sight-threating disease involves oxidative stress.[1,4,16–41] There are multiple classifications of biomarkers related to oxidative stress.[42] In this study, we evaluate sustained presence of free radicals (i.e., a type zero biomarker), an uncontroversial early event in the course of oxidative stress.[1,4,16–42] Sustained production of free radicals can also suppress light-dark hydration changes in the subretinal space that control the distribution of vision-critical neuroprotective molecules such as the interphotoreceptor binding protein; further, it can lead to declines in visual performance.[43–50] However, questions continue regarding whether aged mice show ongoing and excessive production of free radicals in their rods/RPE in vivo and, if so, whether abnormally high levels of free radicals contributes to degradation of vision.

In this study, we address these questions in 2 and 24 mo male C57BL/6J mice. Importantly, the C57BL/6J mouse shows declines in visual performance

after 18 month of age without loss of rod photoreceptors, retinal ganglion cells, or interneurons.[51–55] Mice were studied using the following validated methods to examine the contribution of unremitted production of free radicals and its physiologic consequences. QUEnch-assiSTed (QUEST) magnetic resonance imaging (MRI) measures continuous production of paramagnetic free radicals in retinal laminae in vivo on the basis of a decrease in 1/T1 after acute injection of antioxidants.[40,41,56–58] In the photoreceptor region of the retina, 1/T1 is strongly biased toward rods because it is the dominant cell type in that region.[59] Combining acute antioxidant administration with optical coherence tomography (i.e., QUEST OCT) measures the impact of a constant presence of free radicals on subretinal space thickness, based on whether antioxidants correct an abnormally thin subretinal space in light-adapted mice as measured by the external limiting membrane–retinal pigment epithelium (ELM-RPE) thickness.[43] Combining antioxidant administration with optokinetic tracking (i.e., QUEST OKT) provides a functional assay of vision that is sensitive to unbalenced free radical production based on whether antioxidants re-establish normal cone-based visual performance.[60] Results from these noninvasive assays were compared to a "gold standard" lucigenin assay that measures ex vivo production of superoxide radicals in freshly excised retina, which is biased toward rod cells, the most numerous cell in the retina.[40,41,61,62]

Materials and Methods

All mice were treated in accordance with the National Institutes of Health Guide for the Care and Use of Laboratory Animals, the Association for Research in Vision and Ophthalmology Statement for the Use of Animals in Ophthalmic and Vision Research, and with specific authorization by the Wayne State University Division of Laboratory Animal Resources Institutional Animal and Care Use Committee. Two- and 24-month-old male C57BL/6J mice were obtained from the National Institute of Aging (https://www.nia.nih.gov/research/dab/aged-rodent-colonies-handbook/eligibility-criteria-use-nia-aged-rodent-colonies). They were housed and maintained in 12 hour/12 hour light-dark cycle laboratory lighting for at least a week before study. Mice were humanely euthanized by an overdose of urethane followed by a cervical dislocation, as detailed in our Institutional Animal and Care Use Committee–approved protocol.

The left eye was studied for QUEST MRI, QUEST OCT, and superoxide levels, and both eyes for QUEST OKT. All mice were maintained in darkness overnight. Two assays, QUEST MRI and Lucigenin superoxide measurements, were performed in dark-adapted mice, a condition in which free radical production is high relative to that in the light.[40,56,63] QUEST OCT was performed in mice adapted to five hours' room light (~ 300 lx) because excessive and sustained production of free radicals produces a functional thinning of the ELM-RPE in light-adapted mice but no change in dark-adapted mice.[43,64] Also, QUEST OKT was performed in light-adapted mice to examine cone-based visual performance. QUEST OCT examinations were performed in mice adaptation to room light for five hours to allow time for maximum outer retina thickness expansion.[65] QUEST OKT was performed in mice after at least 15 minutes of room light.[41]

Quest MRI

QUEST MRI is routinely performed in our laboratory and previously described.[40,41,56,66,67] High-resolution MRI data (Fig. 1) were acquired on a 7T system (Bruker ClinScan, Billerica, MA, USA) using a receive-only surface coil (1.0 cm diameter) centered on the left eye. In all groups, immediately before the MRI experiment, animals were anesthetized with urethane (36% solution intraperitoneally; 0.083 mL/20 g animal weight, prepared fresh daily; Sigma–Aldrich, St. Louis, MO, USA) and treated topically with 1% atropine to ensure dilation of the iris followed by 3.5% lidocaine gel to reduce eye motion. MRI data were acquired using several single spin-echo sequences (time to echo 13 ms, 7 × 7 mm^2, matrix size 160 × 320, slice thickness 600 µm). Images were acquired at different repetition times (TR) in the following order (number per time between repetitions in parentheses): TR 0.15 seconds (6), 3.50 seconds (1), 1.00 seconds (2), 1.90 seconds (1), 0.35 seconds (4), 2.70 seconds (1), 0.25 seconds (5), and 0.50 seconds (3). To compensate for reduced signal/noise ratios at shorter TRs, progressively more images were collected as the TR decreased. The present resolution in the central retina is sufficient for extracting meaningful layer-specific anatomic and functional data, as previously demonstrated.[51,64,68]

Antioxidant-injected mice were given 1 mg/kg methylene blue (intraperitoneally, dissolved in saline solution) 24 hours before study and 50 mg/kg α-lipoic acid (intraperitoneally, dissolved in saline and pH adjusted to ~7.4) one hour before study. There is a body of work showing the effectiveness of this methylene blue + α-lipoic acid combination in suppressing the production of free radicals in vivo.[40,41,56,66] Control mice were given two saline solution injections rather than methylene blue and α-lipoic acid.

MRI Data Analysis

As previously described for QUEST MRI data, each T1 data set of 23 images was first processed by registering (rigid body; STACKREG plugin, ImageJ, Rasband, W.S., ImageJ; U. S. National Institutes of Health, Bethesda, MD, USA; https://imagej.nih.gov/ij/, 1997–2016) and then averaging images with the same TRs to generate a stack of eight images.[40,41,56,66] These averaged images were then registered (rigid body) across TRs. QUEST data were corrected for imperfect slice profile bias in the estimate of T1, as previously described [Chapter 18 in reference 69]. Briefly, by normalizing to the shorter TR, some of the bias can be reduced, giving a more precise estimate for T1. To achieve this normalization, we first applied a 3 × 3 Gaussian smoothing (performed three times) on only the TR 150 ms image to minimize noise and emphasize signal. The smoothed TR 150 ms image was then divided into the rest of the images in that T1 data set. Previously, we reported that this procedure helps to minimize day-to-day variation in the 1/T1 profile previously noted and obviated the need for a "vanilla control" group used previously for correcting for day-to-day variations.[40,70] The 1/T1 maps were calculated using the seven normalized images via fitting to a three-parameter T1 equation (y = a + b − (exp(−c − TR)), where a, b, and c are fitted parameters) on a pixel-by-pixel basis using R (v.2.9.0, R Development Core Team [2009], R: A language and environment for statistical computing, R Foundation for Statistical Computing, Vienna, Austria. ISBN 3–900051–07–0) scripts developed in-house, and the minpack.lm

Investigative Ophthalmology & Visual Science

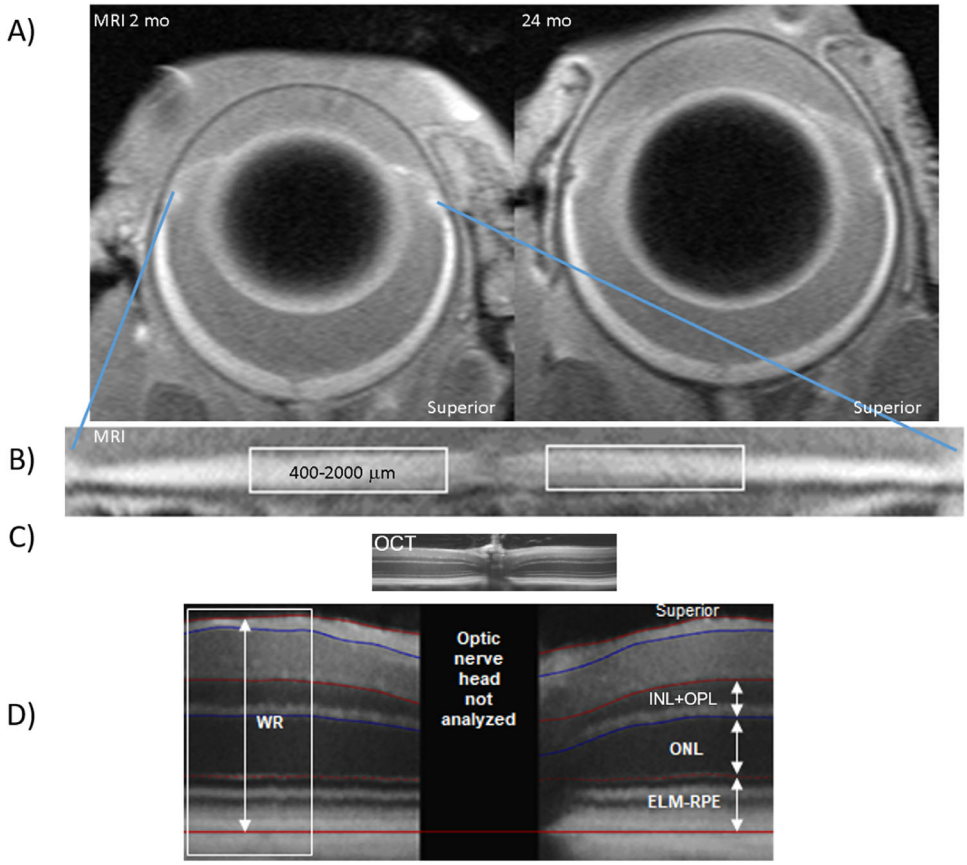

Figure 1. MRI and OCT image analysis regions-of-interest: (**A**) Representative MRI of 2 and 24 mo mouse eyes showing age-related globe growth and retinal thinning; superior side is indicated. No evidence for cataract is noted. (**B**) Representative flattened retina from inferior to superior ciliary bodies (blue lines). Inferior and superior measurement regions-of-interests for MRI data are shown in white boxes. (**C**) Representative OCT for spatial comparison to MRI in B). (**D**) Representative OCT (± 350–630 µm [white box shown on inferior hemiretina, for example]); other laminae measured are also shown bracketed by red and blue lines chosen for visual appreciation. WR, whole retina; INL+OPL, inner nuclear layer + outer plexiform layer.

package (v.1.1.1, Timur V. Elzhov and Katharine M. Mullen minpack.lm: R interface to the Levenberg-Marquardt nonlinear least-squares algorithm found in MINPACK. R package version 1.1–1).

In each mouse, whole retinal thicknesses (µm) were objectively determined using the "half-height method" wherein a border is determined via a computer algorithm on the basis of the crossing point at the midpoint between the local minimum and maximum, as detailed elsewhere.[71,72] The distance between two neighboring crossing-points thus represents an objectively defined retinal thickness. The 1/T1 profiles in each mouse were then normalized with 0% depth at the presumptive vitreoretinal border and 100% depth at the presumptive retina-choroid border.

We separately analyzed superior and inferior profiles from ± 400 to 2000 µm from the optic nerve head (ONH) generated for each animal group (Fig. 1). Excessive and asynchronous production of paramagnetic free radicals in retinal laminae is measured based on a reduction in 1/T1 with methylene blue + α-lipoic acid (i.e., a positive QUEST MRI response).[67]

Retinal Superoxide Production

Superoxide production was measured chemically using a standard and well-validated lucigenin assay (Sigma-Aldrich, St. Louis, MO, USA) and freshly excised retina, as previously described.[40,73] The interaction of Lucigenin and superoxide anion produces a chemiluminescence intensity linearly related to superoxide radical concentration.[74–76] Lucigenin measurements were performed in subgroups of mice maintained in darkness for at least 16 hours. The following day, eyes were removed in the dark, under a dim red light, and retinas were removed under a light dissecting microscope.

Quest OCT

In separate experiments, two- and 24-month-old C57BL/6J mice given saline solution or antioxidants were studied using QUEST OCT.[43] Age-matched C57BL/6 mice dark-adapted overnight and room light-adapted (~300 lx) for five hours the following day, no injections beyond anesthesia. In all groups, OCT (Envisu R2200 VHR SDOIS) was used to measure retinal layer spacing in central retina (Fig. 1) in vivo; note that OCT and MRI interrogate regions with limited spatial overlap (Fig. 1). Mice were anesthetized with urethane (36% solution intraperitoneally; 0.083 mL/20 g animal weight, prepared fresh weekly; Sigma-Aldrich). One percent atropine sulfate was used to dilate the iris, and Systane Ultra was used to lubricate the eyes. Vertical B scan OCT was used in two ways. The first use is to identify retinal layers that contribute to the superior-inferior MRI

Investigative Ophthalmology & Visual Science

profile data since aligning the vitreous-retina (0% depth) and retina-choroid (100% depth) borders of OCT and MRI images reasonably matches structure with function.[77] Second, separate groups of mice were studied in which the optic nerve is positioned to interrogate central superior, and inferior retina (±350–630 µm, Fig. 1). The retinal thicknesses in three layers (i.e., inner nuclear layer + outer plexiform layer [INL+OPL]; outer nuclear layer [ONL]; ELM-RPE) were measured using in-house developed R scripts that objectively identify layer boundaries after searching the space indicated by a hand-drawn estimate ("seed boundaries") (Fig. 1).

Quest OKT

QUEST OKT was performed in separate experiments.[41] Control and antioxidant groups were dark-adapted overnight and light-adapted for between 15 minutes and three hours the following day; initial studies did not find any differences in OKT responses with different light-adaptation times (data not shown). For all groups, two cone-based visual performance metrics were evaluated in awake and freely moving mice using optokinetic tracking: spatial frequency thresholds (SFTs, "acuity", in cycles/degree) and contrast sensitivity (CS, measured near the peak of the nominal curve [0.06 cycles/degree.[78]], inverse Michelson contrast [unitless]) (OptoMotry; CerebralMechanics Inc, Alberta, Canada). In brief, a vertical sine wave grating is projected as a virtual cylinder in three-dimensional coordinate space on computer monitors arranged in a quadrangle around a testing arena. Unrestrained mice (as described above) are placed on an elevated platform at the center of the arena. An experimenter observed a video image of the platform from above to view the animal and follow the position of its head with the aid of a computer mouse and a crosshair continually placed on the mouse head as it moves. The X-Y positional coordinates of the crosshair are centered on the hub of the virtual cylinder, enabling its wall to be maintained at a constant "distance" from the animal's eyes, and thereby fixing the spatial frequency of the stimulus at the animal's viewing position. When the cylinder was rotated in the clockwise or counter-clockwise direction and the animal followed with head and neck movements that tracked the rotation, it was judged whether the animal's visual system could distinguish the grating. Clockwise and counterclockwise tracking provide a measure of left and right eye SFT and CS.[79] Each set of SFT and peak of CS measurements per mouse can reliably be obtained in 30 minutes. We did not measure rod-based visual performance OKT metrics because they are considerably smaller than cone-based OKT indices making them less sensitive to change.[80]

Statistical Analysis

Data are presented as mean and 95% confidence intervals (CI). A significance level of 0.05 was used for all tests. We used generalized linear mixed models with the Kenward-Roger method for calculating degrees of freedom in SAS 9.4 (SAS software, Cary, NC, USA) to analyze all measurements (1/T1, lucigenin, OCT layer thickness, and OKT) because all had multiple measurements for each mouse. 1/T1 is measured along retina depth, resulting in an MRI profile. Likewise, OCT layer thickness is measured along the retina, resulting in a layer thickness profile. For both types of outcomes, we used a linear mixed model with restricted cubic splines to model and compare mouse-specific profiles between groups fit using Proc Mixed in SAS. The number of "windows" (i.e., "knots") with a relationship between outcome (1/T1 or layer thickness) and retina depth/distance from ONH was initially evaluated separately for each group for any given analysis, and the Akaike and Schwarz Bayesian information criteria were used to identify the model with the fewest knots needed to model all groups. Random coefficients for the intercept, side, location-specific coefficients (cubic spline coefficients), and two-way interactions among these effects with mouse nested within age and anti-oxidant treatment were also evaluated using Akaike and Schwarz Bayesian information criteria. Given the random spline coefficients included in all models, we used an unstructured covariance matrix for the random coefficients to account for associations in spline coefficients because of subject-specific profiles.

The final model for 1/T1 used five knots and included random coefficients for the intercept, side, all depth coefficients, and all depth by side interactions. The model included the fixed effects of age, antioxidant treatment, side of the ONL, location-specific values for the cubic splines, and four-way interactions among the main effects. The four-way interaction of age, antioxidant treatment, side, and depth was significant ($P = 0.0080$), indicating that MRI profiles depended on the specific combination of age, treatment, and side. Mean profiles and comparisons of the mean profiles were generated using linear contrasts.

We used a similar modeling strategy for OCT layer thicknesses. The four-way interaction of age, antioxidant treatment, side, and distance from the ONH was significant for all three layers ($P < .0001$). Because the main focus for OCT thickness was on mean thickness across the entire retina, we used linear contrasts to estimate and compare the means averaged over the 350.0 to 624.4 distances. We used this approach to evaluate the effects of age, antioxidant treatment, side, and all interactions on the means averaged over distance. The final model for all layers included random coefficients for side, the sixth spline coefficient for distance from the ONH, and the interaction of side and the sixth spline coefficient. The final model for ELM-RPE, ONL, and INL thickness used eight, eight, and nine knots, respectively.

For the lucigenin assay, superoxide levels were first normalized by dividing by protein concentrations, and then the normalized superoxide levels were log-transformed for analysis using a linear mixed model. The model was fit using Proc Mixed in SAS and included the fixed effect of age and random intercepts for mouse nested within age, day, and for batch nested within day.

For OKT, SFT and contrast sensitivity were analyzed similarly, but assuming different data distributions. We assumed SFT was normally distributed, and we used a gamma-link in a generalized linear mixed model for contrast sensitivity. For both measurements, the model included the fixed effect of group (two months, 24 months saline solution, and 24 months antioxidant), and a random intercept for mouse nested within group. The models were fit using Proc Glimmix in SAS.

Results

Quest MRI

Compared to saline solution–injected controls, the methylene blue + α-lipoic acid combination had no significant

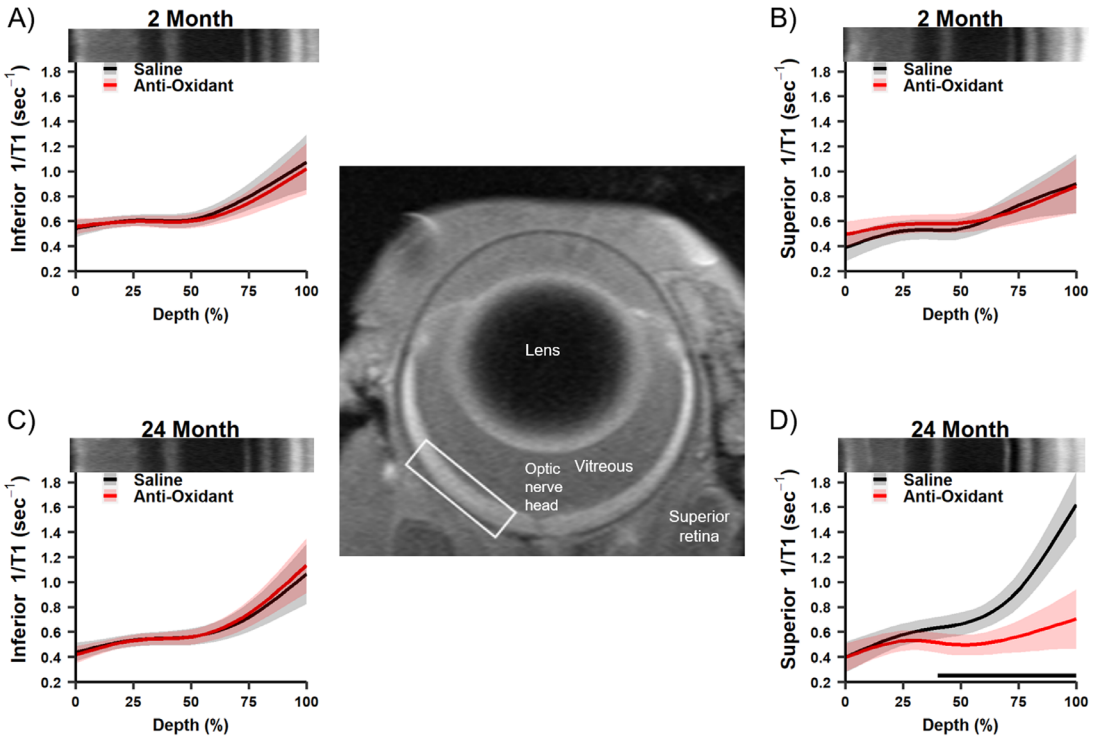

Figure 2. QUEST MRI showing age-related sustained and excessive production of free radicals localized to superior retina: Modeled 1/T1 profiles of dark-adapted (**A, B**) two-month-old and (**C, D**) 24-month-old dark-adapted mice given either saline solution (n = 6, two-month-old mice; n = 5, 24-month-old mice; *black line*) or methylene blue + α-lipoic acid antioxidants (n = 7, two-month-old mice; n = 6, 24-month-old mice; *red line*) measured from 400 to 2000 inferior and superior hemiretina (example of length of region-of-interest shown by *white box*). Representative OCT images from each group are also shown at the top of each graph to indicate laminae locations. Only significant (*horizontal black bar*) antioxidant reduction in 1/T1 indicative of the constant presence of free radicals. Each profile has a *solid line* indicating the mean and a *shaded region* indicating 95% CI.

transretinal impact on 1/T1 of either inferior or superior hemiretina in the two-month group (Fig. 2). On the other hand, in the 24-month group, this antioxidant cocktail significantly ($P < 0.05$) reduced outer retina 1/T1 but only in superior and not inferior hemiretina (Fig. 2).

Lucigenin

Superoxide production in excised retina showed no significant difference between two-month-old mice (mean 235.9; 95% CI, 179.6–310.2) and 24-month-old mice (mean 218.1; 95% CI, 166.1–286.5).

Quest OCT

Retinal thinning with age-related globe growth can be visually appreciated in Figure 1 on MRI examination but did not occur uniformly across layers as measured by OCT (Fig. 3). ELM-RPE was thicker in 24-month-old mice (Figs. 3C, 3I) and showed no significant change after acute injection of antioxidants (Fig. 3F) that were effective in QUEST MRI. In contrast, INL and ONL show thinning with age (Figs. 3A, 3B), and the thinning differed by side. The age effect in INL was statistically significant only on the inferior side (Fig. 3G), and ONL showed greater thinning on the superior side (Fig. 3H). Neither ONL nor INL showed a significant change with antioxidant treatment (Figs. 3D, 3E).

Quest OKT

Older mice had lower cone-based acuity and contrast sensitivity than younger mice ($P < 0.05$). The acute antioxidant protocol that was effective for quenching sustained free radical production as measured by QUEST MRI (Fig. 2) was not effective against age-related declines in vision (Fig. 4).

Discussion

In this study, aged C57BL/6J mice are shown for the first time to exhibit unremitted production of free radicals in the outer retina in vivo as measured by QUEST MRI. This age-related phenomenon exhibited a vertical axis asymmetry that mirrored the reported inferior-superior topology of antioxidant ability in younger mice.[81,82] Interestingly, as humans age, lipofuscin content (a type 1 biomarker of oxidative stress[42]) develops relatively more quickly in superior retina compared to superior retina, and multifocal ERG responses are relatively better preserved in inferior retina.[83–86] We and others have shown that combining antioxidants with photopic OKT allows for the detection of continuous production of retinal free radicals.[38,39,41,87–89] However, as shown herein, administration of antioxidants that are effective per QUEST MRI were ineffective against the declines in vision as measured by QUEST OKT. In addition, QUEST OCT and a Lucigenin assay were both negative for a sustained presence of free radicals. Thus we find little evidence to implicate ongoing uncontrolled production of

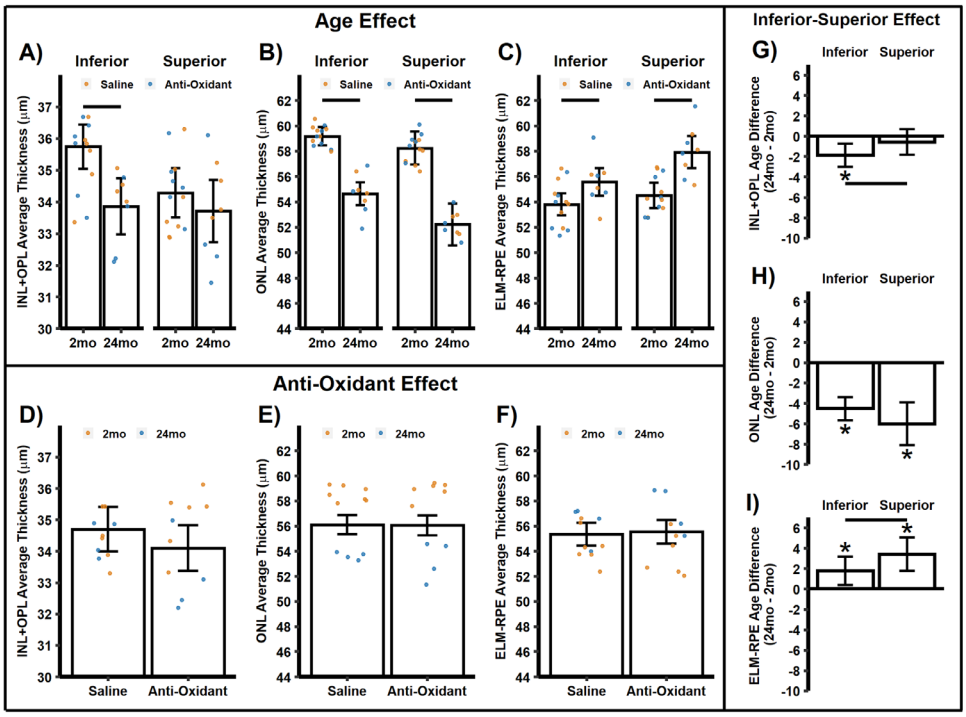

Figure 3. Distinct age-related changes in retinal laminae thickness as measured from OCT images (± 350–630 mm from the optic nerve head) are unrelated to sustained and excessive production of free radicals: (**A, B, C**) Model-based estimates of age differences in thickness for the inner nuclear layer + outer plexiform layer (INL+OPL), ONL, and ELM-RPE region. Each *dot* represents a single mouse datum for the saline solution–treated (*orange*) and antioxidant-treated (*blue*) groups used to generate the average values presented in the *bar graph*. (**D, E, F**) Model-based estimates of antioxidant effects on thickness values for the same three layers. (**G, H, I**) show age differences between inferior and superior retina for each layer. Sample sizes for the four groups of mice are as follows: n = 7, two months old, saline solution; n = 6, two months old, antioxidant; n = 4, 24 months old, saline solution; n = 4, 24 months old, antioxidant. Each *dot* represents a single mouse datum for the two-month-old (*orange*) and 24-month-old (*blue*) groups used to generate the average values presented in the *bar graph*. Significant thickness differences are indicated by the horizontal black bar; the star indicates differences from zero. *Error bars*: 95% CI.

outer retina free radicals in vivo in 24-month-old C57BL/6J mice in reductions in visual performance.

Importantly, the biophysical sensitivity of QUEST MRI to sustained superoxide production has been demonstrated in phantoms of the xanthine/xanthine oxidase reaction or in solutions of KO_2.[58,90] In mice, the noninvasive free radical readout of QUEST MRI under physiologic conditions has also been validated against gold-standard ex vivo assays during dark and light adaptation of (i) rods and (ii) cones, and (iii) in postnatal day seven mice that have anatomical but not yet functioning rods.[40,56] Finally, the accuracy of QUEST MRI as a type zero biomarker of oxidative stress has been confirmed to be a reliable measure of ongoing production of free radicals in excess of antioxidant defenses in the retina in several mouse models including (i) after the RPE-toxin sodium iodate, (ii) in RPE-specific MnSOD knockout mice, (iii) in diabetes, (iv) in phosphodiesterase 6b knockout mice, and (v) after pharmaceutical inhibition of phosphodiesterase 6.[40–42,50,56,61] Conventional markers (e.g., type one biomarkers[42]) are measured from excised tissue and measure downstream consequences of excessive free radical production, such as lipid peroxides, or oxidative damage to DNA (oxoguanosine); these type one biomarkers can be confounded by variable/unreported postmortem intervals.[61,91,92] The antioxidant combination used herein is based on its effectiveness in the above studies and was indeed demonstrated to be effective in vivo as measured by QUEST MRI (Fig. 2).[40,41,50,56,61] It is likely, however, that other antioxidants will also be effective in vivo, although those studies remain to be done. On the basis of the above body of work and considerations, QUEST MRI is an accurate, stand-alone in vivo assay for addressing questions regarding the continuous and excessive production of free radicals in vivo.

We were somewhat surprised by the apparent lack of agreement between QUEST MRI and QUEST OCT and Lucigenin. One possible reason for these different outcomes is that QUEST MRI reports on the continuous production of all free radical species during data collection. In contrast, Lucigenin is a assay specific for superoxide free radical content. QUEST OCT may be less sensitive to excessive production of free radical species other than superoxide but this idea is so far untested. These considerations raise the possibility that the free radical species that contribute to the positive QUEST MRI results was not superoxide but other reactive oxygen species, such as H_2O_2 or hydroxyl free radical. In support for this hypothesis, we note that aged C57BL/6J accumulate iron in their RPE, a condition associated with H_2O_2/hydroxyl-evoked production of free radicals.[10] Free radical production localized to just RPE can produce extensive and sustained production of free radicals in the rest of the outer retina.[56] Rod outer segments are reported to show an ectopic oxidative phosphorylation pathway and ex vivo studies have shown that this system can produce reactive oxygen intermediates, although it is uncertain whether production of a particular free radical species

Investigative Ophthalmology & Visual Science

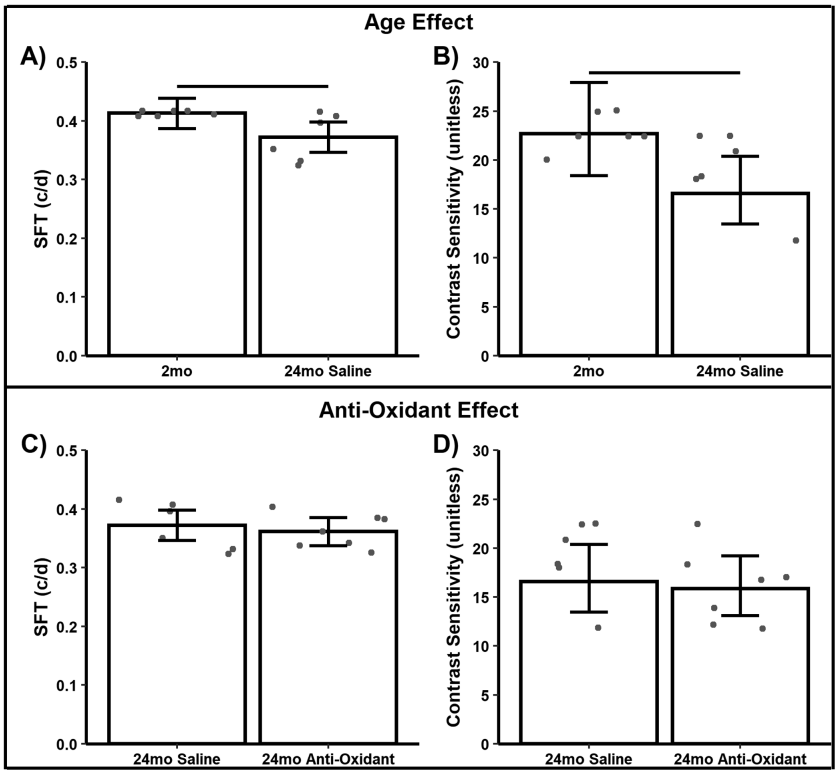

Figure 4. Visual performance declines in 24-month-old mice are unaffected by antioxidants. (**A, B**) Age and (**C, D**) antioxidant effects on SFT (cycles/degree; i.e., acuity) and presumptive peak of contrast sensitivity curve from two- and 24-month-old mice (n = 4, two months old, saline solution; n = 6, 24 months old, saline solution; n = 7, 24 months old, antioxidant). Each dot represents a single mouse datum used to generate the average values presented in the bar graph. *Error bars*: CI. *Black horizontal bar*: $P \leq 0.05$.

dominates.[93,94] Also, it is unclear whether the topology of RPE or ectopic sources of free radicals mirror the inferior and superior retina differences in production of free radicals that are measured in 24-month-old mice (Fig. 2). More work is needed to understand the spatiotemporal evolution of non-superoxide free radicals in two- and 24-month-old C57BL/6J mice.

Age-related visual performance decline is also thought to arise from rod photoreceptor death during "healthy" aging, a possible downstream consequence of a constant presence of free radicals.[11,95–97] Aging C57BL/6J mice show outer nuclear layer thinning with age (Fig. 3B), although this thinning does not appear to be due to rod death. For example, a significant rod-dominated ONL thinning was not associated with significant ELM-RPE thinning in this study, which might be expected if a sufficiently large number of rods were degenerating. These data support results in the literature that C57BL/6J mice maintain a constant number of photoreceptors, retinal ganglion cells, and interneurons as they age with the retina expanding as the globe matures thus maintaining retinal volume; rhodopsin levels (a biomarker of rod content) appear constant up to 17 months of age.[53,98] In addition, we note that in rats, retinal volume remained steady with age.[96,99] In older humans, rod density declines without a reduction in rhodopsin content, which would be predicted to occur from loss of rods, the most numerous cell in the retina.[11,100] In short, there is little evidence to support the occurrence of rod photoreceptor death during healthy aging of C57BL/6J mice.

So what could be responsible for the age-related ONL thinning? We considered three possibilities. First, ONL thinning is linked to an increase in the size of the eye with age, which can be visually appreciated in Figure 1.[53] Yet, globe growth per se is expected to affect both INL and ONL to similar degrees. This prediction, however, was not borne out by the present data in Figure 3 suggesting the contribution of other factors. Second, the observed ONL thinning was due to cone death.[101] One subpopulation of cone cells in peripheral inferior retina has been reported to selectively undergo death by 12 months of age in C57Bl/6J mice.[101] However, cones make up only ~3% of the total photoreceptor population in the mouse and so the reported localized loss of a fraction of 3% does not seem to account for the panretinal ONL thinning in central retina in Figure 3.[59] Furthermore, the reported cone loss at 12 months does not appear to be physiologically meaningful because cone-based visual performance is maintained in C57BL/6J mice until 18 months.[51,52,89,102]

A third possibility for ONL thinning involves age-related accumulation of activated microglia within the subretinal space.[30,103] If microglia density in the subretinal space becomes high enough it might mechanically compress the ONL causing thinning.[103] It is unknown whether such thinning per se is linked with diminished vision with age. We also note that the secretory ability of activated microglia is controlled by different L-type calcium channels (LTCC; e.g., Cav1.2 and Cav1.3) and that it has been reported that an increase in LTCC activity in the outer retina of aging rats (as measured by manganese-enhanced MRI) is predictive of reduced vision with age; the role of a particular Cav1.* LTCC in C57BL/6J mice is less studied.[96,104,105] It is unclear whether the increased LTCC activity with age is a causative

factor for vision declines with age or an indirect biomarker of subretinal space microglia/outer nuclear layer thinning. More work is needed to unravel these notions.

This study had three major limitations. First, only male mice were studied, and sex is an important biological variable that was not considered. Similar studies are needed in female mice. Second, the design was cross-sectional. However, the results for each assay were derived from two or more separate groups of mice and good reproducibility (i.e., low data scatter, see Figures) was noted within groups. Third, we did not start giving antioxidants before visual performance declines (i.e., before 18 months), so the present data do not address the question of whether sustained free radical presence (either in the retina or in postretinal pathways) played an early causative role.[51] More work is needed to test this notion. In summary, first-in-kind evidence in vivo does not support the hypothesis that ongoing uncontrolled production of outer retina free radicals in vivo causes reductions in visual performance in 24-month-old C57BL/6J mice.

Acknowledgments

The authors thank HoaHua Qian for his comments and insight, and David Bissig for ongoing R scripts and development. We also thank Brennan Schilling and Arthur Orchanian for their help during the early stages of manuscript preparation.

Supported by the National Institutes of Health [RO1 EY026584 (BAB) and R01 AG058171 (BAB)], NEI Core Grant P30 EY04068, and an unrestricted grant from Research to Prevent Blindness (Kresge Eye Institute, BAB).

Disclosure: **B.A. Berkowitz**, None; **R.H. Podolsky**, None; **K.L. Childers**, None; **R. Roberts**, None; **M. Schneider**, None; **E. Graffice**, None; **K. Sinan,** None; **A. Berri**, None; **L. Harp**, None

References

1. Spear PD. Neural bases of visual deficits during aging. *Vis Res*. 1993;33:2589–2609.
2. Swindell W, Ensrud K, Cawthon P, et al. Indicators of "healthy aging" in older women (65–69 years of age). A data-mining approach based on prediction of long-term survival. *BMC Geriatrics*. 2010;10:55.
3. Ardeljan D, Chan C-C. Aging is not a disease: distinguishing age-related macular degeneration from aging. *Prog Retin Eye Res*. 2013;37:68–89.
4. Parapuram SK, Cojocaru RI, Chang JR, et al. Distinct signature of altered homeostasis in aging rod photoreceptors: implications for retinal diseases. *PLoS One*. 2010;5:e13885.
5. Sachdeva MM, Cano M, Handa JT. Nrf2 signaling is impaired in the aging RPE given an oxidative insult. *Exp Eye Res*. 2014;119:111–114.
6. Handa JT. How does the macula protect itself from oxidative stress? *Mol Aspects Med*. 2012;33:418–435.
7. Bonnel S, Mohand-Said S, Sahel JA. The aging of the retina. *Exp Gerontol*. 2003;38:825–831.
8. Curcio CA, Medeiros NE, Millican CL. Photoreceptor loss in age-related macular degeneration. *Invest Ophthalmol Vis Sci*. 1996;37:1236–1249.
9. Seo SJ, Krebs MP, Mao H, Jones K, Conners M, Lewin AS. Pathological consequences of long-term mitochondrial oxidative stress in the mouse retinal pigment epithelium. *Exp Eye Res*. 2012;101:60–71.
10. Hahn P, Song Y, Ying G-s, He X, Beard J, Dunaief JL. Age-dependent and gender-specific changes in mouse tissue iron by strain. *Exp Gerontol*. 2009;44:594–600.
11. Curcio CA, Millican CL, Allen KA, Kalina RE. Aging of the human photoreceptor mosaic: evidence for selective vulnerability of rods in central retina. *Invest Ophthalmol Vis Sci*. 1993;34:3278–3296.
12. Asteriti S, Gargini C, Cangiano L. Mouse rods signal through gap junctions with cones. *Elife*. 2014;3:e01386.
13. Qiao S-N, Zhang Z, Ribelayga CP, Zhong Y-M, Zhang D-Q. Multiple cone pathways are involved in photic regulation of retinal dopamine. *Sci Rep*. 2016;6:28916–28916.
14. Aung MH, Hn Park, Han MK, et al. Dopamine Deficiency Contributes to Early Visual Dysfunction in a Rodent Model of Type 1 Diabetes. *J Neurosci*. 2014;34:726–736.
15. Azimipour M, Migacz JV, Zawadzki RJ, Werner JS, Jonnal RS. Functional retinal imaging using adaptive optics swept-source OCT at 1.6MHz. *Optica*. 2019;6:300–303.
16. Muralidharan P, Cserne Szappanos H, Ingley E, Hool L. Evidence for redox sensing by a human cardiac calcium channel. *Sci Rep*. 2016;6:19067.
17. Hool LC. The L-type Ca^{2+} channel as a potential mediator of pathology during alterations in cellular redox state. *Heart Lung Circ*. 2009;18:3–10.
18. Perron NR, Beeson C, Rohrer B. Early alterations in mitochondrial reserve capacity: a means to predict subsequent photoreceptor cell death. *J Bioenerg Biomembr*. 2013;45:101–109.
19. Bonilha VL, Bell BA, Rayborn ME, et al. Absence of DJ-1 causes age-related retinal abnormalities in association with increased oxidative stress. *Free Radic Biol Med*. 2017;104:226–237.
20. El-Sayyad HI, Khalifa SA, El-Sayyad FI, Mousa SA, Mohammed EA. Analysis of fine structure and biochemical changes of retina during aging of Wistar albino rats. *Clin Exp Ophthalmol*. 2014;42:169–181.
21. Pinazo-Duran MD, Gallego-Pinazo R, Garcia-Medina JJ, et al. Oxidative stress and its downstream signaling in aging eyes. *Clin Interv Aging*. 2014;9:637–652.
22. Gu X, Neric NJ, Crabb JS, et al. Age-related changes in the retinal pigment epithelium (RPE). *PLoS One*. 2012;7:e38673.
23. Liang FQ, Godley BF. Oxidative stress-induced mitochondrial DNA damage in human retinal pigment epithelial cells: a possible mechanism for RPE aging and age-related macular degeneration. *Exp Eye Res*. 2003;76:397–403.
24. Hahn P, Ying GS, Beard J, Dunaief JL. Iron levels in human retina: sex difference and increase with age. *Neuroreport*. 2006;17:1803–1806.
25. Wang AL, Lukas TJ, Yuan M, Neufeld AH. Age-related increase in mitochondrial DNA damage and loss of DNA repair capacity in the neural retina. *Neurobiol Aging*. 2010;31:2002–2010.
26. Barron MJ, Johnson MA, Andrews RM, et al. Mitochondrial abnormalities in ageing macular photoreceptors. *Invest Ophthalmol Vis Sci*. 2001;42:3016–3022.
27. Wang AL, Lukas TJ, Yuan M, Neufeld AH. Increased mitochondrial DNA damage and down-regulation of DNA repair enzymes in aged rodent retinal pigment epithelium and choroid. *Mol Vis*. 2008;14:644–651.
28. Kim C-S, Park S, Chun Y, Song W, Kim H-J, Kim J. Treadmill exercise attenuates retinal oxidative stress in naturally-aged mice: an immunohistochemical study. *Int J Mol Sci*. 2015;16:21008–21020.
29. Zhao L, Feng Z, Zou X, Cao K, Xu J, Liu J. Aging leads to elevation of O-GlcNAcylation and disruption of mitochondrial homeostasis in retina. *Oxid Med Cell Longev*. 2014;2014:425705.

30. Xu H, Chen M, Forrester JV. Para-inflammation in the aging retina. *Prog Retin Eye Res*. 2009;28:348–368.
31. De La Paz M, RE Anderson. Region and age-dependent variation in susceptibility of the human retina to lipid peroxidation. *Invest Ophthalmol Vis Sci*. 1992;33:3497–3499.
32. Nag TC, Kumar P, Wadhwa S. Age related distribution of 4-hydroxy 2-nonenal immunoreactivity in human retina. *Exp Eye Res*. 2017;165:125–135.
33. Nag TC, Wadhwa S, Alladi PA, Sanyal T. Localization of 4-hydroxy 2-nonenal immunoreactivity in aging human retinal Muller cells. *Ann Anat*. 2011;193:205–210.
34. Kubo E, Chhunchha B, Singh P, Sasaki H, Singh DP. Sulforaphane reactivates cellular antioxidant defense by inducing Nrf2/ARE/Prdx6 activity during aging and oxidative stress. *Sci Rep*. 2017;7:14130.
35. Bonilha VL, Bell BA, Rayborn ME, et al. Loss of DJ-1 elicits retinal abnormalities, visual dysfunction, and increased oxidative stress in mice. *Exp Eye Res*. 2015;139:22–36.
36. Gorusupudi A, Nelson K, Bernstein PS. The Age-Related Eye Disease 2 Study: micronutrients in the treatment of macular degeneration. *Adv Nutr*. 2017;8:40–53.
37. Rohrer B, Bandyopadhyay M, Beeson C. Reduced metabolic capacity in aged primary retinal pigment epithelium (rpe) is correlated with increased susceptibility to oxidative stress. In: Bowes Rickman C, LaVail MM, Anderson RE, Grimm C, Hollyfield J, Ash J (eds), *Retinal Degenerative Diseases*. Cham: Springer International Publishing; 2016:793–798.
38. Patel AK, Hackam AS. A novel protective role for the innate immunity toll-like receptor 3 (TLR3) in the retina via Stat3. *Mol Cell Neurosci*. 2014;63:38–48.
39. Berkowitz BA, Kern TS, Bissig D, et al. Systemic retinaldehyde treatment corrects retinal oxidative stress, rod dysfunction, and impaired visual performance in diabetic mice. *Invest Ophthalmol Vis Sci*. 2015;56:6294–6303.
40. Berkowitz BA, Bredell BX, Davis C, Samardzija M, Grimm C, Roberts R. Measuring in vivo free radical production by the outer retina. *Invest Ophthalmol Vis Sci*. 2015;56:7931–7938.
41. Berkowitz BA, Podolsky RH, Lenning J, et al. Sodium iodate produces a strain-dependent retinal oxidative stress response measured in vivo using QUEST MRI. *Invest Ophthalmol Vis Sci*. 2017;58:3286–3293.
42. Ghezzi P. Environmental risk factors and their footprints in vivo—a proposal for the classification of oxidative stress biomarkers. *Redox Biol*. 2020;34:101442.
43. Berkowitz BA, Podolsky RH, Lins-Childers KM, Li Y, Qian H. Outer retinal oxidative stress measured in vivo using QUEnch-assiSTed (QUEST) OCT. *Invest Ophthalmol Vis Sci*. 2019;60:1566–1570.
44. Uehara F, Yasumura D, LaVail MM. Development of light-evoked changes of the interphotoreceptor matrix in normal and RCS rats with inherited retinal dystrophy. *Exp Eye Res*. 1991;53:55–60.
45. Uehara F, Matthes MT, Yasumura D, LaVail MM. Light-evoked changes in the interphotoreceptor matrix. *Science*. 1990;248:1633–1636.
46. Chen C, Adler L, Goletz P, Gonzalez-Fernandez F, Thompson DA, Koutalos Y. Interphotoreceptor retinoid–binding protein removes all-trans-retinol and retinal from rod outer segments, preventing lipofuscin precursor formation. *J Biol Chem*. 2017;292:19356–19365.
47. Lee M, Li S, Sato K, Jin M. Interphotoreceptor retinoid-binding protein mitigates cellular oxidative stress and mitochondrial dysfunction induced by all-trans-retinal. *Invest Ophthalmol Vis Sci*. 2016;57:1553–1562.
48. Sun Z, Zhang M, Liu W, Tian J, Xu G. Photoreceptor IRBP prevents light induced injury. *Front Biosci (Landmark Ed)*. 2016;21:958–972.
49. Mieziewska K. The interphotoreceptor matrix, a space in sight. *Microsc Res Tech*. 1996;35:463–471.
50. Berkowitz BA, Podolsky RH, Lenning J, et al. Sodium iodate produces a strain-dependent retinal oxidative stress response measured in vivo using QUEST MRI. *Invest Ophthalmol Vis Sci*. 2017;58:3286–3293.
51. Berkowitz BA, Grady EM, Roberts R. Confirming a prediction of the calcium hypothesis of photoreceptor aging in mice. *Neurobiol Aging*. 2014;35:1883–1891.
52. Lehmann K, Schmidt KF, L+¦wel S. Vision and visual plasticity in ageing mice. *Restor Neurol Neurosci*. 2012;30:161–178.
53. Samuel MA, Zhang Y, Meister M, Sanes JR. Age-related alterations in neurons of the mouse retina. *J Neurosci*. 2011;31:16033–16044.
54. Trachimowicz RA, Fisher LJ, Hinds JW. Preservation of retinal structure in aged pigmented mice. *Neurobiol Aging*. 1981;2:133–141.
55. Li C, Cheng M, Yang H, Peachey NS, Naash MI. Age-Related Changes in the Mouse Outer Retina. *Optom Vis Sci*. 2001;78:425–430.
56. Berkowitz BA, Lewin AS, Biswal MR, Bredell BX, Davis C, Roberts R. MRI of retinal free radical production with laminar resolution in vivo. *Invest Ophthalmol Vis Sci*. 2016;57:577–585.
57. Stinnett G, Moore K, Samuel E, et al. A novel assay for the in vivo detection of reactive oxygen species using MRI. *ISMRM Meeting Abstracts*. 2015;1917.
58. Berkowitz BA, Lenning J, Khetarpal N, et al. In vivo imaging of prodromal hippocampus CA1 subfield oxidative stress in models of Alzheimer disease and Angelman syndrome. *FASEB J*. 2017;31:4179–4186.
59. Carter-Dawson LD, Lavail MM, Sidman RL. Differential effect of the rd mutation on rods and cones in the mouse retina. *Invest Ophthalmol Vis Sci*. 1978;17:489–498.
60. Berkowitz BA, Kern TS, Bissig D, et al. Systemic retinaldehyde treatment corrects retinal oxidative stress, rod dysfunction, and impaired visual performance in diabetic mice systemic retinaldehyde treatment in diabetic mice. *Invest Ophthalmol Vis Sci*. 2015;56:6294–6303.
61. Berkowitz BA, Podolsky RH, Berri AM, et al. Dark rearing does not prevent rod oxidative stress in vivo in Pde6brd10 mice. *Invest Ophthalmol Vis Sci*. 2018;59:1659–1665.
62. Jeon CJ, Strettoi E, Masland RH. The major cell populations of the mouse retina. *J Neurosci*. 1998;18:8936–8946.
63. Kern TS. Do photoreceptor cells cause the development of retinal vascular disease? *Vis Res*. 2017;139:65–71.
64. Berkowitz BA, Grady EM, Khetarpal N, Patel A, Roberts R. Oxidative stress and light-evoked responses of the posterior segment in a mouse model of diabetic retinopathy. *Invest Ophthalmol Vis Sci*. 2015;56:606–615.
65. Li Y, Fariss RN, Qian JW, Cohen ED, Qian H. Light-induced thickening of photoreceptor outer segment layer detected by ultra-high resolution OCT imaging. *Invest Ophthalmol Vis Sci*. 2016;57:Oct105–111.
66. Berkowitz BA, Podolsky RH, Farrell B, et al. D-cis-diltiazem can produce oxidative stress in healthy depolarized rods in vivo. *Invest Ophthalmol Vis Sci*. 2018;59:2999–3010.
67. Berkowitz BA. Oxidative stress measured in vivo without an exogenous contrast agent using QUEST MRI. *J Magn Reson*. 2018;291:94–100.
68. Berkowitz BA, Bissig D, Roberts R. MRI of rod cell compartment-specific function in disease and treatment in vivo. *Prog Retin Eye Res*. 2016;51:90–106.

Investigative Ophthalmology & Visual Science

69. Haacke EM, Brown RW, Thompson MR, Venkatesan R. *Magnetic Resonance Imaging: Physical Principles and Sequence Design*: Hoboken, NJ: Wiley; 1999.
70. Berkowitz BA, Lewin AS, Biswal MR, Bredell BX, Davis C, Roberts R. MRI of retinal free radical production with laminar resolution in vivo free radical production with laminar resolution in vivo. *Invest Ophthalmol Vis Sci*. 2016;57:577–585.
71. Bissig D, Berkowitz BA. Same-session functional assessment of rat retina and brain with manganese-enhanced MRI. *Neuroimage*. 2011;58:749–760.
72. Cheng H, Nair G, Walker TA, et al. Structural and functional MRI reveals multiple retinal layers. *Proc Natl Acad Sci USA*. 2006;103:17525–17530.
73. Li Y, Zhu H, Kuppusamy P, Roubaud V, Zweier JL, Trush MA. Validation of lucigenin (bis-N-methylacridinium) as a chemilumigenic probe for detecting superoxide anion radical production by enzymatic and cellular systems. *J Biol Chem*. 1998;273:2015–2023.
74. Gyllenhammar H. Lucigenin chemiluminescence in the assessment of neutrophil superoxide production. *J Immunol Methods*. 1987;97:209–213.
75. Du Y, Miller CM, Kern TS. Hyperglycemia increases mitochondrial superoxide in retina and retinal cells. *Free Radic Biol Med*. 2003;35:1491–1499.
76. Vladimirov YA, Proskurnina EV. Free radicals and cell chemiluminescence. *Biochemistry (Mosc)*. 2009;74:1545–1566.
77. Berkowitz BA, Bissig D, Roberts R. MRI of rod cell compartment-specific function in disease and treatment in-vivo. *Prog Retin Eye Res*. 2016;51:90–106.
78. Prusky GT, Alam NM, Beekman S, Douglas RM. Rapid quantification of adult and developing mouse spatial vision using a virtual optomotor system. *Invest Ophthalmol Vis Sci*. 2004;45:4611–4616.
79. Douglas RM, Alam NM, Silver BD, McGill TJ, Tschetter WW, Prusky GT. Independent visual threshold measurements in the two eyes of freely moving rats and mice using a virtual-reality optokinetic system. *Vis Neurosci*. 2005;22:677–684.
80. Alam NM, Altimus CM, Douglas RM, Hattar S, Prusky GT. Photoreceptor regulation of spatial visual behavior photoreceptor-mediated visual function. *Invest Ophthalmol Vis Sci*. 2015;56:1842–1849.
81. Zhu Y, Natoli R, Valter K, Stone J. Differential gene expression in mouse retina related to regional differences in vulnerability to hyperoxia. *Mol Vis*. 2010;16:740–755.
82. Williams MA, Pinto LH, Gherson J. The retinal pigment epithelium of wild type (C57BL/6J +/+) and pearl mutant (C57BL/6J pe/pe) mice. *Invest Ophthalmol Vis Sci*. 1985;26:657–669.
83. Tzekov RT, Gerth C, Werner JS. Senescence of human multifocal electroretinogram components: a localized approach. *Graefes Arch Clin Exp Ophthalmol*. 2004;242:549–560.
84. Delori FC, Goger DG, Dorey CK. Age-related accumulation and spatial distribution of lipofuscin in RPE of normal subjects. *Invest Ophthalmol Vis Sci*. 2001;42:1855–1866.
85. Gray DA, Woulfe J. Lipofuscin and aging: a matter of toxic waste. *Sci Aging Knowl Environ*. 2005;2005:re1-.
86. Sohal RS, Brunk UT. Lipofuscin as an indicator of oxidative stress and aging. *Adv Exp Med Biol*. 1989;266:17–26; discussion 27–19.
87. Jackson CR, Ruan GX, Aseem F, et al. Retinal dopamine mediates multiple dimensions of light-adapted vision. *J Neurosci*. 2012;32:9359–9368.
88. Franco LM, Zulliger R, Wolf-Schnurrbusch UE, et al. Low dose sodium iodate induces patchy loss of retinal pigment epithelium and decreases visual function in a mouse model. *Invest Ophthalmol Vis Sci*. 2009;50:4004–4010.
89. Cahill H, Nathans J. The optokinetic reflex as a tool for quantitative analyses of nervous system function in mice: application to genetic and drug-induced variation. *PLoS One*. 2008;3:e2055.
90. MacKinnon MJ, Berkowitz BA, Shih YI. Superoxide free radical spin-lattice relaxivity: A quench-assisted MR study. *Magn Reson Med*. 2021;86:1058–1066.
91. Cheng G, Zielonka M, Dranka B, et al. Detection of mitochondria-generated reactive oxygen species in cells using multiple probes and methods: potentials, pitfalls, and the future. *J Biol Chem*. 2018;293:10363–10380.
92. Xiao Y, Meierhofer D. Are Hydroethidine-Based Probes Reliable for Reactive Oxygen Species Detection? *Antioxid Redox Signal*. 2019;31:359–367.
93. Bruschi M, Bartolucci M, Petretto A, et al. Differential expression of the five redox complexes in the retinal mitochondria or rod outer segment disks is consistent with their different functionality. *FASEB BioAdvances*. 2020;2:315–324.
94. Bruschi M, Petretto A, Caicci F, et al. Proteome of Bovine Mitochondria and Rod Outer Segment Disks: Commonalities and Differences. *J Proteome Res*. 2018;17:918–925.
95. Sivapathasuntharam C, Sivaprasad S, Hogg C, Jeffery G. Improving mitochondrial function significantly reduces the rate of age related photoreceptor loss. *Exp Eye Res*. 2019;185:107691.
96. Bissig D, Goebel D, Berkowitz BA. Diminished Vision in Healthy Aging Is Associated with Increased Retinal L-Type Voltage Gated Calcium Channel Ion Influx. *PLoS One*. 2013;8:e56340.
97. Cunea A, Jeffery G. The ageing photoreceptor. *Vis Neurosci*. 2007;24:151–155.
98. Gresh J, Goletz PW, Crouch RK, Rohrer B. Structure-function analysis of rods and cones in juvenile, adult, and aged C57bl/6 and Balb/c mice. *Vis Neurosci*. 2003;20:211–220.
99. Feng L, Sun Z, Han H, Zhou Y, Zhang M. No age-related cell loss in three retinal nuclear layers of the Long-Evans rat. *Vis Neurosci*. 2007;24:799–803.
100. Fulton AB, Dodge J, Hansen RM, Williams TP. The Rhodopsin Content of Human Eyes. *Invest Ophthalmol Vis Sci*. 1999;40:1878–1883.
101. Cunea A, Powner MB, Jeffery G. Death by color: differential cone loss in the aging mouse retina. *Neurobiol Aging*. 2014;35:2584–2591.
102. Kolesnikov AV, Fan J, Crouch RK, Kefalov VJ. Age-Related Deterioration of Rod Vision in Mice. *J Neurosci*. 2010;30:11222–11231.
103. Xu H, Chen M, Manivannan A, Lois N, Forrester JV. Age-dependent accumulation of lipofuscin in perivascular and subretinal microglia in experimental mice. *Aging Cell*. 2008;7:58–68.
104. Wang X, Saegusa H, Huntula S, Tanabe T. Blockade of microglial Cav1.2 Ca(2+) channel exacerbates the symptoms in a Parkinson's disease model. *Sci Rep*. 2019;9:9138–9138.
105. Espinosa-Parrilla JF, Martínez-Moreno M, Gasull X, Mahy N, Rodríguez MJ. The L-type voltage-gated calcium channel modulates microglial pro-inflammatory activity. *Mol Cell Neurosci*. 2015;64:104–115.

Investigative Ophthalmology & Visual Science